Mon. Not. R. Astron. Soc. **389,** 141–155 (2008) doi:10.1111/j.1365-2966.2008.13516.x

Massive stars exploding in a He-rich circumstellar medium – III. SN 2006jc: infrared echoes from new and old dust in the progenitor CSM

S. Mattila,[⋆1,2] W. P. S. Meikle,[3] P. Lundqvist,[4] A. Pastorello,[1] R. Kotak,[1] J. Eldridge,[5] S. Smartt,[1] A. Adamson,[6] C. L. Gerardy,[7] L. Rizzi,[6] A. W. Stephens[8] and S. D. Van Dyk[9]

[1]*Astrophysics Research Centre, School of Mathematics and Physics, Queen's University, Belfast BT7 1NN*
[2]*Tuorla Observatory, University of Turku, Väisäläntie 20, FI-21500 Piikkiö, Finland*
[3]*Astrophysics Group, Blackett Laboratory, Imperial College London, Prince Consort Road, London SW7 2AZ*
[4]*Department of Astronomy, Stockholm University, AlbaNova, SE-106 91 Stockholm, Sweden*
[5]*Institute of Astronomy, The Observatories, University of Cambridge, Madingley Road, Cambridge CB3 0HA*
[6]*Joint Astronomy Centre, 660 North A'ohoku Place, Hilo, HI 96720, USA*
[7]*Department of Physics, Florida State University, Tallahassee, FL 32306, USA*
[8]*Gemini Observatory, 670 North A'ohoku Place, Hilo, HI 96720, USA*
[9]*Spitzer Science Centre/Caltech, Pasadena, CA 91125, USA*

Accepted 2008 May 26. Received 2008 May 26; in original form 2008 March 14

ABSTRACT

We present near- (NIR) and mid-infrared (MIR) photometric data of the Type Ibn supernova (SN) 2006jc obtained with the United Kingdom Infrared Telescope (UKIRT), the Gemini North Telescope and the *Spitzer Space Telescope* between days 86 and 493 post-explosion. We find that the IR behaviour of SN 2006jc can be explained as a combination of IR echoes from two manifestations of circumstellar material. The bulk of the NIR emission arises from an IR echo from newly condensed dust in a cool dense shell (CDS) produced by the interaction of the ejecta outward shock with a dense shell of circumstellar material ejected by the progenitor in a luminous blue variable (LBV)-like outburst about two years prior to the SN explosion. The CDS dust mass reaches a modest 3.0×10^{-4} $M_{\odot}$ by day 230. While dust condensation within a CDS formed behind the ejecta inward shock has been proposed before for one event (SN 1998S), SN 2006jc is the first one showing evidence for dust condensation in a CDS formed behind the ejecta outward shock in the circumstellar material. At later epochs, a substantial and growing contribution to the IR fluxes arises from an IR echo from pre-existing dust in the progenitor wind. The mass of the pre-existing circumstellar medium (CSM) dust is at least $\sim 8 \times 10^{-3}$ $M_{\odot}$. This paper therefore adds to the evidence that mass-loss from the *progenitors* of core-collapse SNe could be a major source of dust in the Universe. However, yet again, we see no direct evidence that the explosion of an SN produces anything other than a very modest amount of dust.

Key words: circumstellar matter – supernovae: general – supernovae: individual: SN 2006jc – dust, extinction.

1 INTRODUCTION

The importance of core-collapse supernovae (CCSNe) as a source of cosmic dust is currently a highly debated topic. For several decades it has been hypothesized that the physical conditions in the expanding SN ejecta could result in the condensation of large amounts of dust (e.g. Cernuschi, Marsicano & Codina 1967; Hoyle & Wickramasinghe 1970; Gehrz 1989; Tielens 1990; Dwek 1998). More recently, CCSNe arising from Population III stars have been proposed as the main source of dust in the early Universe (Todini & Ferrara 2001; Nozawa et al. 2003; Dwek, Galliano & Jones 2007). Models of dust formation in CCSNe (Todini & Ferrara 2001; Nozawa et al. 2003, 2008) succeed in producing large amounts of dust that would be enough to account for the dust seen at high redshifts (see Meikle et al. 2007). However, direct observational evidence for CCSNe as a major source of dust is still missing, even in the local Universe (Meikle et al. 2007 and references therein).

SN 2006jc was discovered on 2006 October 9.75 UT by Nakano et al. (2006) in the nearby spiral galaxy UGC 4904 and was classified as a peculiar Type Ib SN (Benetti et al. 2006; Crotts et al. 2006;

⋆E-mail: s.mattila@utu.fi

Modjaz et al. 2006). The SN was discovered after optical maximum. However, model fits to the bolometric light curve (Pastorello et al. 2008a) yielded the most satisfactory fits with an explosion date of 2006 September 21 ($JD = 245\,4000$). In the following paper we shall adopt this date as epoch $t = 0$. Comparison with the earlier discovered SN 1999cq suggests that optical maximum occurred at about +84 to +10 d (Pastorello et al. 2008a). The early-time SN shows an apparently hybrid spectrum with broad emission lines of intermediate-mass elements commonly observed in Type Ic SNe and relatively narrow [full width at half-maximum (FWHM) ∼2000–3000 km s^{-1}] emission lines of helium originating from a dense circumstellar medium (CSM) around the SN (Foley et al. 2007; Pastorello et al. 2007). The He I lines were already apparent in the first spectrum obtained at ∼20 d and persisted until at least 180 d (Pastorello et al. 2008a). In addition, SN 2006jc showed Hα emission with a narrower profile indicating an origin in a different CSM region from that which gave rise to the He lines. Excess emission in both ultraviolet (UV) and X-rays (Brown, Immler & Modjaz 2006; Immler, Modjaz & Brown 2006; Immler et al. 2008) also indicates the presence of a substantial CSM. It appears that SN 2006jc actually belongs to a subclass of Type Ic events which show evidence of a dense He-rich CSM. Other examples are SNe 1999cq and 2002ao (Matheson et al. 2000; Foley et al. 2007; Pastorello et al. 2008a), SN 2000er (Pastorello et al. 2008a) and SN 2005la which appear to be a transitional case between SN 2006jc-like events and Type IIn SNe (Pastorello et al. 2008b). A new classification as Type Ibn has been proposed (Pastorello et al. 2007, 2008a) for such SN 2006jc-like events.

An outburst similar to those exhibited by the most energetic luminous blue variables (LBVs) was detected at the SN 2006jc location two years before its explosion (Nakano et al. 2006; Pastorello et al. 2007). Foley et al. (2007) and Pastorello et al. (2007) suggested that a helium-rich shell was ejected during this event and that this shell is giving rise to the He I lines. The apparent LBV-like outburst indicates that the progenitor of both the outburst and SN 2006jc might have been a very massive star (Foley et al. 2007; Pastorello et al. 2007, 2008a). Alternatively, SN 2006jc could have originated in a binary system consisting of an LBV that erupted in 2004, and a Wolf–Rayet star that gave rise to SN 2006jc (Pastorello et al. 2007, 2008a).

SN 2006jc has provided also the first ever opportunity of observing dust formation associated with this subtype of CCSN. Dust production associated with SNe can be studied via the thermal infrared (IR) emission from the grains, or by their attenuating effect on light passing through the dusty regions. Near-IR (NIR) excesses have been observed in five Type IIn SNe and five other Type II subtypes (e.g. Fassia et al. 2000; Di Carlo et al. 2002; Gerardy et al. 2002). However, prior to SN 2006jc, only in three examples of non-Type II CCSNe have NIR excesses been reported: SN 1982E (probable Type Ib, Graham & Meikle 1986), SN 1982R (Type Ib, Graham 1985; Graham & Meikle 1986) and SN 2002ic (peculiar event, Kotak et al. 2004). The attenuation method has been applied to the Type IIpec SN 1987A (e.g. Danziger et al. 1989; Lucy et al. 1989), the Type Ib SN 1990I (Elmhamdi et al. 2004), the Type IIn SN 1998S (Pozzo et al. 2004) and the Type IIP SNe 1999em (Elmhamdi et al. 2003) and 2003gd (Sugerman et al. 2006).

As early as +55 d, SN 2006jc had already developed a strong NIR excess (Arkharov et al. 2006; Minezaki, Yoshii & Nomoto 2007; Smith, Foley & Filippenko 2008). Observations by Di Carlo et al. (2008) and by us (see below) show that the NIR excess peaked at around 80 d and persisted to past 200 d. Sakon et al. (2008) report NIR and mid-IR (MIR) observations at 220 d, confirming the persistence of the IR excess to at least this epoch. We confirm this, and find that the IR excess persisted to at least 493 d. In addition, optical observations reported by Smith et al. (2008) and by us show that the narrow He I lines became systematically blueshifted after ∼50 d and that over the same period an abrupt steepening was observed in the optical light curves. The optical light curves of SN 2006jc are also analysed by Di Carlo et al. (2008), Tominaga et al. (2008) and Pastorello et al. (2008a).

A study of the IR excess in SN 2006jc was first presented by Smith et al. (2008). Subsequent papers discussing the IR excess include those of Sakon et al. (2008), Tominaga et al. (2008), Di Carlo et al. (2008), Nozawa et al. (2008) and the present paper. Smith et al., Di Carlo et al. and the work presented here all propose dust formation in an outward shock-formed cool dense shell (CDS) to account for the NIR emission. In contrast, Sakon et al., Tominaga et al. and Nozawa et al. propose dust formation in the SN ejecta. The idea of dust formation in a CDS in the CCSN context was originally introduced by Pozzo et al. (2004) to account for the IR and optical behaviour of SN 1998S. SN 2006jc provides the second opportunity to study this phenomenon. Therefore, to investigate the origin of the IR excess in SN 2006jc, we commenced an NIR and MIR photometric monitoring campaign via Director's Discretionary Time (DDT) on the United Kingdom Infrared Telescope (UKIRT) and the Gemini North Telescope, and Target of Opportunity (ToO) observations with the *Spitzer Space Telescope* (*Spitzer*).

In this paper, we examine the presence of newly formed dust in SN 2006jc via both its IR emission and its attenuating effects on the optical emission. Using a more extensive IR data set than presented in previous studies, plus modelling of the shock interaction, we confirm the proposition of Smith et al. and Di Carlo et al. of the dust formation in a CDS and strengthen the support for it. In addition, we show (i) how absorption and reradiation by the CDS dust of the early-time UV/optical emission from the SN (i.e. an IR echo) can provide a self-consistent explanation for the bulk of the NIR luminosity and evolution and (ii) that a second, cooler IR echo also occurred due to dust in the undisturbed progenitor CSM. Optical observations and a systematic study of the observed properties of SN 2006jc and the four other Type Ibn events are presented in two companion papers (Pastorello et al. 2008a,b).

2 INFRARED OBSERVATIONS

SN 2006jc was observed in the *JHK* bands with the WFCAM wide-field NIR imager on UKIRT at eight epochs between 2006 December 16 (epoch +86 d) and 2007 May 10 (epoch +231 d). At each epoch, five dithered images were acquired with the SN placed both in the north-west and south-east corners of one of the WFCAM detectors. The data were reduced and photometrically calibrated via the WFCAM pipeline at the Cambridge Astronomical Survey Unit (CASU). A *K*-band observation was also obtained with the UFTI NIR imager on UKIRT on 2007 June 27 (epoch +279 d).

Seven months later, on 2008 January 27 (epoch +493 d), a deep 3840-s on-source integration was obtained with the NIRI NIR imager on the Gemini North Telescope under the DDT programme GN-2007B-DD-8. The jittered on-source frames were sky subtracted using the IRAF XDIMSUM package and were median-combined, excluding a few frames with less successful sky subtraction. The final combined image has a seeing FWHM of ∼0.45 arcsec. The photometric calibration utilized a nearby photometric standard (FS 127) observed immediately after the SN. To identify the SN location we aligned a combined (2007 April 26 and May 10) UKIRT

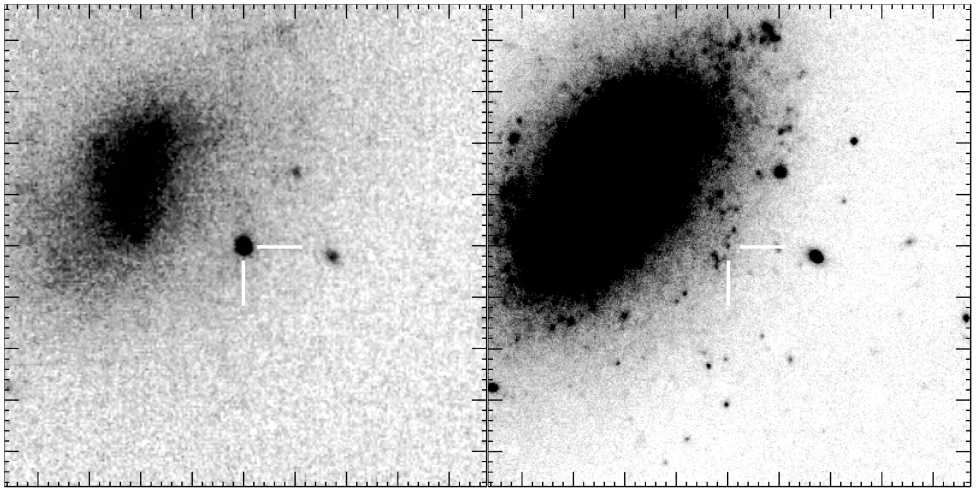

Figure 1. The field of SN 2006jc at 2.2 μm. The field of view (FOV) of the image is 47 × 47 arcsec^2 and the SN (marked with ticks) is located in the middle. The left-hand image was obtained by combining UKIRT images from 2007 April 26 and May 10. The right-hand image is a deep integration obtained at Gemini on 2008 January 27. North is up and east is to the left-hand side.

K-band image with the Gemini image. For this procedure, 15 point-like sources common to the two images were used to obtain a general geometric transformation (with no distortion term), yielding an rms of 0.03 and 0.02 arcsec in *x* and *y*, respectively. The aligned UKIRT image and the deep Gemini image are shown in Fig. 1. A faint point source is present in the Gemini image coincident with the SN position.

SN 2006jc was also observed with the *Spitzer*'s Infrared Array Camera (IRAC) at 3.6, 4.5, 5.8 and 8.0 μm on 2007 May 7 (epoch +228 d) and November 25 (epoch +430 d) within *Spitzer* programmes PID 30292 and 40619. The pre-explosion field of SN 2006jc was also serendipitously observed within the Spitzer Infrared Nearby Galaxies Survey (SINGS) (PID: 0159; Kennicutt et al. 2003) at 3.6 and 5.8 μm on 2004 April 30. We used the post-basic calibrated data (PBCD) products provided by the S16.1.0 version of the *Spitzer* pipeline in this study. The pre- and post-explosion (2007 May 7) 5.8-μm IRAC images are shown in Fig. 2.

3 INFRARED PHOTOMETRY OF SN 2006JC

Aperture photometry was performed on the two sets of UKIRT *JHK* images obtained at each epoch, using the Starlink package *GAIA* (Draper, Gray & Berry 2002). A 3.0 arcsec radius aperture was used for all except the latest epochs, where a 2.0 arcsec radius aperture was used to yield more accurate photometry when the SN was faint relative to the host galaxy. The sky was measured within a 1.5–2.0 × radius annulus. Aperture correction in each image was carried out via large-aperture photometry of three nearby bright stars (2MASS J09173378+4153251, J09172752+4153381 and J09170785+4152504 in the *J* and *H* bands, and J09173181+4151543, J09172752+4153381 and J09170557+4154505 in the *K* band). The magnitudes of the stars were compared with their average values (over all the epochs) to check and if necessary adjust the photometric calibration produced by the CASU pipeline. We also compared these magnitudes with those available from 2MASS and found that they agreed within 0.06, 0.02 and 0.02 mag in *J, H* and *K* bands, respectively. Finally, the average of the two measurements at each epoch was adopted as the SN magnitude. The statistical error in the SN photometry and the standard deviation of the recalibrated field star magnitudes were added in quadrature to yield the uncertainty in each measurement. The resulting SN photometric measurements are listed in Table 1.

To measure the SN magnitude in the Gemini *K*-band image we performed point spread function (PSF) fitting using the SNOOPY[1] package based on IRAF's DAOPHOT. For this measurement the SN position was fixed according to the centroid coordinates obtained from the aligned UKIRT image where the SN was still bright. The photometric uncertainty was estimated via PSF fitting to artificial sources placed close to the SN position after subtracting the PSF fit at the SN position. This yielded a *K*-band magnitude of 21.64 ± 0.40 for the SN.

GAIA was also used to perform aperture photometry on the SN in the *Spitzer* IRAC images. A 2.25 arcsec radius aperture was used and the sky was measured within a 1.5–2.0 × radius annulus. This aperture was chosen as a compromise between maximizing the sampled fraction of the source flux (the radius of the first diffraction minimum at the extreme red end of the 8.0-μm channel is 2.6 arcsec) and minimizing any extended residual emission in the subtracted images (see below). Aperture corrections were derived from the IRAC PSF images available on the *Spitzer* web site. The correction factors were 1.23, 1.26, 1.50 and 1.65 for 3.6, 4.5, 5.8

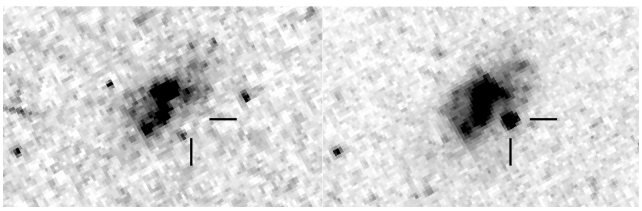

Figure 2. The field of SN 2006jc at 5.8 μm. The FOV of the image is 107 × 77 arcsec^2 and the SN location is marked with ticks. The images were obtained with IRAC on *Spitzer* on 2004 April 30 (left-hand side) and 2007 May 7 (right-hand side). North is up and east is to the left-hand side.

[1] SNOOPY, originally presented in Patat (1996), has been implemented in IRAF by E. Cappellaro. The package is based on DAOPHOT, but optimized for SN magnitude measurements.

Table 1. UKIRT WFCAM (days 86–231), UKIRT UFTI (day 279) and Gemini NIRI (day 493) NIR magnitudes and *Spitzer* IRAC (days 228 and 430) MIR fluxes of SN 2006jc. The SN epochs (rounded to the nearest whole number) are relative to the estimated explosion date, JD = 245 4000 (Pastorello et al. 2008a). Uncertainties are shown in brackets. For completeness, we also tabulate the NIR photometry of Arkharov et al. (2006) used in our analysis. We note that more recently Di Carlo et al. (2008) have also reported updated photometry based on the data set used by Arkharov et al.

Date (UT)	JD 240 0000	Epoch (d)	*J*	*H*	*K*	Source
2006 November 15	54054.55	55	15.87	15.64	15.01	Arkharov et al.
2006 November 16	54055.55	56	–	15.53	–	Arkharov et al.
2006 November 24	54063.55	64	15.93	15.47	14.64	Arkharov et al.
2006 December 03	54072.54	73	15.92	15.08	14.29	Arkharov et al.
2006 December 06	54075.54	76	15.88	15.01	14.20	Arkharov et al.
2006 December 16	54085.97	86	15.83(0.01)	14.76(0.01)	13.87(0.01)	This paper
2006 December 23	54093.00	93	16.01(0.01)	14.86(0.01)	13.91(0.01)	This paper
2006 December 30	54099.88	100	16.28(0.01)	15.04(0.01)	14.00(0.01)	This paper
2007 January 13	54113.92	114	16.85(0.02)	15.43(0.01)	14.27(0.01)	This paper
2007 January 20	54121.00	121	17.08(0.02)	15.63(0.01)	14.40(0.01)	This paper
2007 March 16	54175.93	176	19.25(0.15)	17.23(0.04)	15.56(0.03)	This paper
2007 April 26	54216.73	217	–	18.17(0.08)	16.39(0.03)	This paper
2007 May 10	54230.74	231	–	18.49(0.12)	16.67(0.05)	This paper
2007 June 27	54278.74	279	–	–	17.60(0.10)	This paper
2008 January 27	54492.97	493	–	–	21.64(0.40)	This paper
			3.6 μm	4.5 μm	5.8 μm	8.0 μm
2007 May 7	54227.54	228	506 ± 3 μJy	632 ± 7 μJy	727 ± 7 μJy	707 ± 11 μJy
2007 November 25	54429.67	430	49 ± 2 μJy	92 ± 10 μJy	199 ± 6 μJy	286 ± 10 μJy

and 8.0 μm, respectively. The contribution of background flux to these results was assessed through the use of image subtraction. At 3.6 and 5.8 μm, we subtracted the pre-explosion SINGS images from our post-explosion PBCD-processed images using image matching and subtraction techniques as implemented in the ISIS 2.2 image-subtraction package (Alard 2000). In Meikle et al. (2006), we demonstrated the applicability of the image-subtraction technique for *Spitzer*/IRAC SN data and assessed its uncertainties. For SN 2006jc, we found that for day +228 the fluxes measured in the subtracted frames were about 5 per cent lower than in the unsubtracted images. However, no point source was apparent in the IRAC pre-explosion images at the SN location (see Fig. 2), such as might have been produced by the presumably dusty CSM of the SN progenitor system that also gave rise to the LBV-like outburst in 2004. We conclude that the flux difference was due to diffuse, irregular background emission. A similar excess was found in the day 430 5.8-μm unsubtracted image. However, at 3.6 μm the excess was about 50 per cent. The fluxes obtained from the subtracted images were adopted as the true SN fluxes. At 4.5 and 8.0 μm the true fluxes were estimated by scaling downward the values from the unsubtracted images. The shift was 5 per cent for all except the second epoch 4.5-μm observation where we imposed a shift of 25 per cent, this being a rough interpolation between the adjacent band shifts. The resulting MIR fluxes are listed in Table 1.

4 ANALYSIS

4.1 Evidence for dust from the IR spectral energy distribution

To explore the evidence for dust we make use of our IR photometry (see Table 1) and the optical photometry of Pastorello et al. (2007, 2008a). We use also the *JHK* measurements of Arkharov et al. (2006) which cover epochs 55–76 d (Table 1), when the NIR light curves of SN 2006jc were still rising [we note that more recently Di Carlo et al. (2008) have also reported photometry based on the Arkharov et al. data set]. To take an initially neutral standpoint on the interpretation, we have compared blackbodies (see Fig. 3) with the optical to NIR spectral energy distribution (SED) at each epoch between 55 and 231 d, for which at least *H*- and *K*-band data were available.

The optical photometric data were interpolated to the epochs of the NIR observations. The data at each epoch are compared with combined hot and warm blackbodies. The parameter value evolution is presented in Table 2 and Fig. 4. The optical part is represented by a hot (10 000–15 000 K) blackbody, presumably due to the hot photosphere of the SN, and the IR part by a warm (1050–1850 K) blackbody. The warm blackbody is adjusted to optimize the match to the *HK* points only. This was done since contamination by line emission could be relatively greater in the *J* band. In practice, by about 100 d the *J* points were generally also well reproduced by the *HK*-matched blackbodies. The warm blackbody temperature stayed around 1800 K for several weeks before declining to ∼1000 K by day 231. Its radius increased to about 0.8×10^{16} cm by day 176 and then declined. This corresponds to a blackbody velocity of ∼7000–8000 km s^{-1} between 55 and 140 d (see Fig. 4). The luminosity of the warm component peaked around 90 d after which it faded. The contribution of the hot component was dominant at day 55 (>90 per cent of the total luminosity) but by day ∼80, the warm component luminosity exceeded that of the hot component and by day 217, the hot component was less than 1 per cent of the warm component.

A single blackbody was unable to reproduce both the NIR fluxes at 231 d and the MIR fluxes at 228 d. It is unlikely that this was due to the slightly different epochs. We therefore added a third (cold) blackbody component to account for the MIR fluxes, and the warm + cold blackbody combination is illustrated in Fig. 3 as a dotted line. A single cold blackbody reproduced the day 430 NIR/MIR SED (Fig. 3) where the *K*-band point was obtained by interpolation between the days 279 and 493 observations. Owing to the uncertainty in this procedure an error of ±0.7 mag was assigned

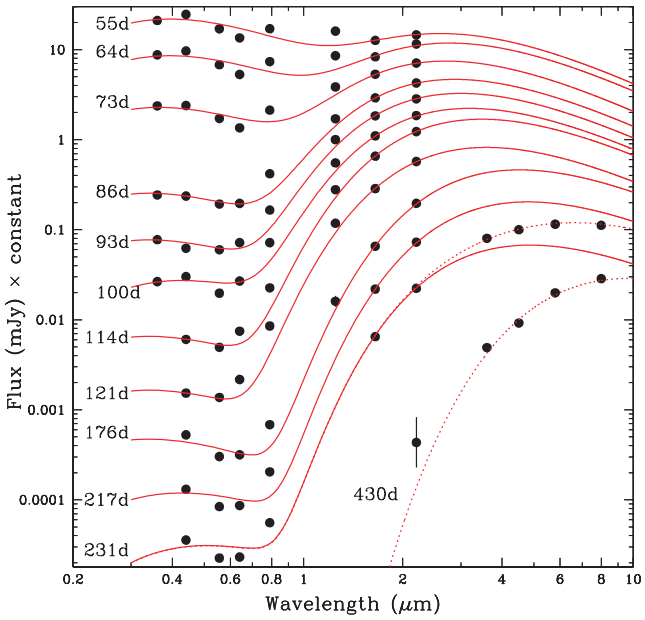

Figure 3. Two-component blackbodies compared with the optical–NIR SEDs of SN 2006jc between 55 and 231 d (see Table 2). The blackbodies have been reddened according to the Cardelli et al. (1989) extinction law with $A_V = 0.15$ (Pastorello et al. 2007). The IR data between 55 and 73 d are from Arkharov et al. (2006) and the rest of the data are from this study. The optical data are from Pastorello et al. (2007, 2008a) and have been interpolated to the epochs of the IR observations. The epochs are relative to the estimated explosion epoch at JD = 245 4000 (Pastorello et al. 2008a). The dotted lines show that the MIR component at 231 d and the NIR and MIR components at 430 d can be reproduced by adding cool blackbodies (see Table 3). The plots have been shifted vertically for clarity.

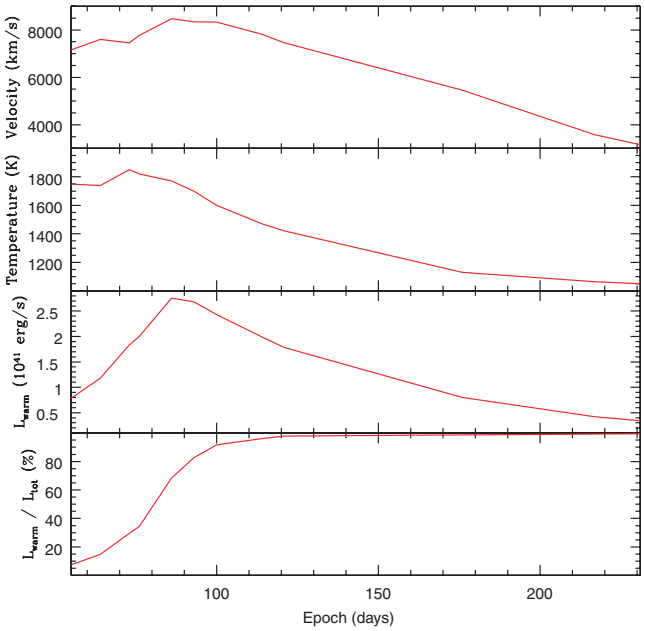

Figure 4. Evolution of the parameter values of the warm blackbodies matched to the *H* and *K* fluxes of SN 2006jc (Table 2). The blackbody velocities were obtained by dividing the blackbody radii by the epochs of the observations.

to the interpolated point. The parameter values for days 228/31 and 430 warm and cold blackbodies are given in Table 3. On day 228/31 the luminosity of the warm component exceeded that of the cold by a factor of ∼2.

Given the temperatures, sizes and luminosities of the warm and cold blackbodies plus the evolution of the warm component, the most plausible explanation for these components of the SED is thermal emission from dust in the SN ejecta and/or in the surrounding medium. A similar conclusion was reached by Smith et al. (2008), as well as by Sakon et al. (2008), Tominaga et al. (2008), Di Carlo et al. (2002) and Nozawa et al. (2008). Further interpretation requires us to address the location and energy source of the radiating dust. We shall consider IR emission from newly formed dust in the ejecta and/or in a shell formed by the interaction of the SN ejecta with circumstellar material. We shall also consider emission from pre-existing dust in the progenitor wind.

4.2 Evidence for new dust from line profiles and light curves

We sought evidence of newly formed dust via the optical line profiles. Fig. 5 illustrates the evolution of the profiles of the narrow He I and Hα lines using data from Pastorello et al. (2007, 2008a). The He I lines show a clear blueshift which increased to ∼600 km s^{-1} between ∼60 and ∼100 d. Over the same period,

Table 2. Parameter values of the hot and warm blackbodies matched to the optical to the *H* and *K* fluxes of SN 2006jc.

Epoch (d)	Radius dust (10^{16}cm)	Temperature dust (K)	Luminosity dust (10^{40} erg s^{-1})	Radius hot (10^{14} cm)	Temperature hot (K)	Luminosity hot (10^{40} erg s^{-1})	Luminosity total (10^{40} erg s^{-1})	L_{hot}/L_{tot} (per cent)
55	0.34	1750	7.82	2.18	13 000	97.3	105.1	92.6
64	0.42	1740	11.80	1.82	13 000	67.8	79.6	85.2
73	0.47	1850	18.33	1.26	14 000	43.6	61.9	70.4
76	0.51	1820	20.00	1.18	14 000	38.2	58.2	65.6
86	0.63	1770	27.57	0.59	15 000	12.7	40.3	31.5
93	0.67	1700	26.79	0.39	15 000	5.59	32.4	17.3
100	0.72	1600	24.31	0.39	12 000	2.23	26.5	8.4
114	0.77	1470	19.89	0.15	15 000	0.79	20.7	3.8
121	0.78	1420	17.81	0.10	15 000	0.38	18.2	2.1
176	0.83	1130	7.98	0.055	15 000	0.108	8.09	1.3
217	0.67	1065	4.18	0.043	12 000	0.027	4.21	0.64
231	0.63	1050	3.44	0.046	10 000	0.015	3.44	0.44

Table 3. Parameter values of the warm and cold blackbody matches to the days 228/31 and 430 SEDs (see Fig. 3).

	Temperature (K)	Radius (cm)	Luminosity (erg s^{-1})
Day 228/31			
Warm blackbody	1050	0.63×10^{16}	3.44×10^{40}
Cold blackbody	620	1.34×10^{16}	1.89×10^{40}
Total luminosity			5.33×10^{40}
Day 430			
Cold blackbody	520	1.5×10^{16}	1.17×10^{40}

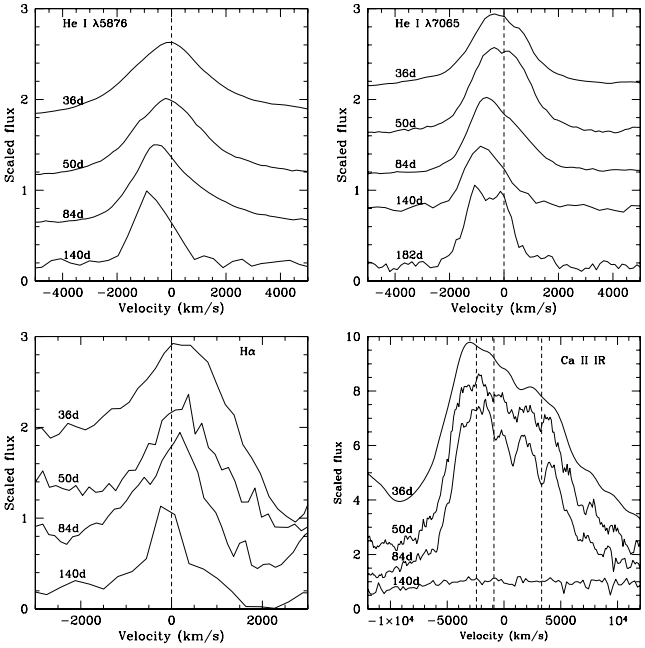

Figure 5. Evolution of the spectral line profiles of He I λ5876 and λ7065 and Hα in velocity space. The evolution of the Ca II IR triplet profile is also illustrated. The velocities are with respect to the average wavelength of the three lines. The zero velocities (with respect to the host galaxy recession velocity) are marked by vertical dashed lines.

Smith et al. (2008) also found the He I lines becoming progressively more asymmetric and blueshifted. Concurrently, the width of the line profile decreased. The FWHM of the He I λ7065 line decreased from ∼2400 to ∼1800 km s^{-1} between 54 and 96 d. There is less convincing evidence for a blueshift in the narrow Hα line. There may be a modest shift between 84 and 140 d but the signal-to-noise ratio is low. Over the same period, Smith et al. (2008) find that the Hα profile is not systematically shifted to the blue. Blueshifts observed in broad SN lines, e.g. in the case of SN 1987A, have been attributed to dust condensation in the SN ejecta (e.g. Danziger et al. 1989; Lucy et al. 1989). Similar evidence for dust has been reported for SNe 1999em and 1990I (Elmhamdi et al. 2003, 2004), SN 1998S (Pozzo et al. 2004) and SN 2003gd (Sugerman et al. 2006). However, such blueshifts were not observed in the broad lines of SN 2006jc. Instead, the broad lines simply disappeared by 140 d (see Fig. 5). In contrast, the narrow He I lines persisted until at least 182 d. A detection of He II λ4686 emission was reported by Smith et al. (2008), appearing some time between days 71 and 95 and disappearing between 122 and 148 d. Our closest observation

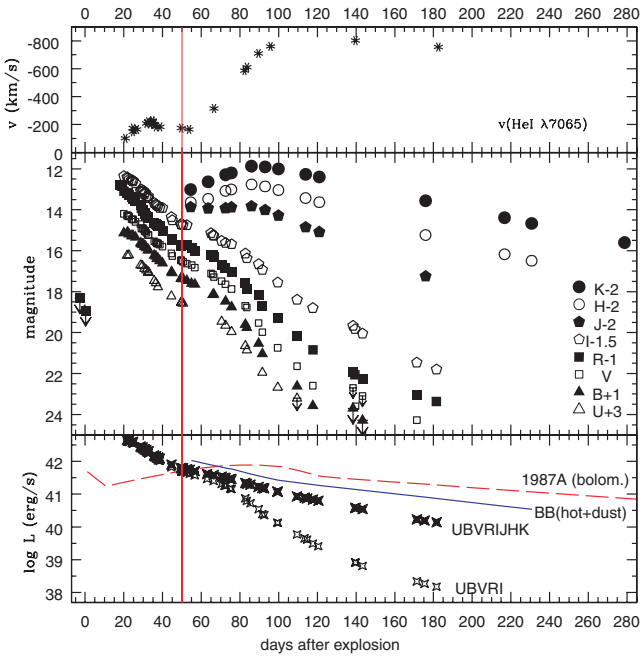

Figure 6. Top: The velocity of the line centre of He I λ7065 with respect to the rest wavelength as a function of the SN epoch (data are from Pastorello et al. 2007, 2008a). Middle: Optical (Pastorello et al. 2007, 2008a) and NIR light curves of SN 2006jc. Bottom: Optical (*U* to *I*) and optical + NIR (*U* to *K*) quasi-bolometric light curves of SN 2006jc (Pastorello et al. 2008a). Also shown is the bolometric light curve of SN 2006jc obtained by summing the hot and warm component blackbody luminosities at each epoch (Table 2). In addition, the bolometric (*U* to *M* band) light curve of SN 1987A (Suntzeff & Bouchet 1990) is plotted for comparison. The day 50 epoch is indicated in each panel as a vertical line. This is the approximate date at which we deduce that dust condensation commenced (see text).

epochs to these were at 88 and 132 d but no sign of He II λ4686 emission was found. It is conceivable that our observations did not cover the period when the He II emission was strong. In Fig. 6 we compare the evolution of the He I λ7065 line centre in velocity space (top panel) with the optical and NIR light curves of the SN (middle panel). It can be seen that the He I line blueshift started to develop at about the same time as the NIR excess appeared. This supports the proposal of Smith et al. (2008) (see also Sakon et al. 2008, Tominaga et al. 2008, Di Carlo et al. 2008 and Nozawa et al. 2008) that the NIR excess is indeed due to local dust condensation. We also note that, as Smith et al. point out, the Ca II triplet line (Fig. 5) simply fades, and does not show the characteristic blueshift of He I lines.

We also examined the individual light curves for indications of dust formation. At about 65 d (10 d after the first evidence of an IR excess) an abrupt steepening of the *UVBRI* light curves can be seen. The steeper slopes persist until about 120 d. The steepening becomes more pronounced as we move to shorter wavelengths, although this reddening is not a strong effect. Relative to the slopes seen in the period 50–65 d, the additional attenuation by day 120 is quite substantial, namely roughly $A_B = 3.0$, $A_V = 2.8$, $A_R = 2.8$, $A_I = 1.8$. We propose that the slope steepening is due to attenuation by newly formed dust. The lack of strong wavelength dependence may be due to the dust forming in clumps rather than in a uniform distribution.

We have also created optical and optical + NIR 'quasi-bolometric' light curves (quasi-BLCs) by integrating over the SN

SED between *U* and *I* bands and *U* and *K* bands, respectively, at each epoch (see Pastorello et al. 2008a for details). Zero flux was assumed at the blue edge of the *U* band and at the red edge of the *I* or *K* band. It is important to note that this procedure implicitly assumes that the optical and NIR fluxes have contemporary energy sources. If a significant fraction of the NIR arose from an IR echo then, owing to light traveltime effects, simple addition of the optical and IR fluxes might not give a meaningful quasi-BLC unless the distance of the reradiating dust from the ejecta was small enough (see Sections 4.4 and 4.5). The quasi-BLCs are shown in the bottom panel of Fig. 6 as open and filled stars, respectively. The optical quasi-BLC exhibits a steepening relative to the optical + NIR BLC, thus supporting the dust condensation hypothesis. It might be argued that, since the *U* to *K* BLC does not include photospheric emission shortward of the *U* band nor dust emission longward of the *K* band, it does not give a true picture of the SN's bolometric evolution (see also Pastorello et al. 2008a). We therefore created a more realistic BLC by summing the luminosities of the hot and warm blackbody components at each epoch (see Table 2). The resulting BLC is shown in Fig. 6, bottom panel. At 55 d, the blackbody-based BLC luminosity exceeds that of the *U* to *K* BLC by about $\times 2$, rising to $\times 6$ by 200 d. At early times this is due to the contribution of the unobserved UV emission shortward of the *U* band and at later times the growing IR contribution beyond the *K* band (see Fig. 3). We note that the optical quasi-BLC also shows steepening relative to this blackbody-based BLC. We conclude that the light curves provide evidence of dust formation in the SN 2006jc vicinity. For comparison the *U*- to *M*-band BLC of SN 1987A (Suntzeff & Bouchet 1990) is also shown in Fig. 6. We note that the post-130-d BLC of SN 2006jc has roughly a third of the luminosity of SN 1987A's BLC. This is in spite of the estimated ^{56}Ni mass (Pastorello et al. 2008a; Tominaga et al. 2008) being $\times 3$–6 greater. The explanation for this is the (possibly) much lower ejecta mass, together with the higher ($\sim \times 5$) ejecta velocity of SN 2006jc. Consequently the gamma-ray transparency of the SN 2006jc ejecta increases much more rapidly. The BLCs of SN 2006jc will be used in Sections 4.4–4.7 as input luminosities for IR echo models. The day 50 epoch is indicated in each panel as a vertical line. This is the approximate date at which we deduce that dust condensation commenced (see below).

4.3 Newly formed dust in the ejecta?

For newly formed ejecta dust to attain the warm blackbody radii given in Table 2, the blackbody radius must have expanded at about 8000 km s^{-1} up to $\sim$120 d (see also Fig. 4). A similarly high blackbody velocity ($\sim$7000 km s^{-1}) is required for the cold component in the three-blackbody match at 228/31 d (see Table 3). In more typical CCSNe, such velocities would imply that much of the IR emission could not have been due to newly formed dust in the SN ejecta as there are not enough suitable refractory elements available for dust condensation at such high velocities. For example, the nebular spectrum of the Type IIP SN 2003gd indicated that the bulk of the metals lay at velocities below $\sim$2000 km s^{-1} (Hendry et al. 2005). However, higher metal velocities are found in other SN types. In particular, Type Ic SNe exhibit nebular metal velocities of 5000–8000 km s^{-1} (Filippenko et al. 1995; Taubenberger et al. 2006). Despite the fact that the latest spectrum available for SN 2006jc (183 d) (Pastorello et al. 2008a) shows no sign of nebular metal lines, the probable origin of the SN in a star lying on the Ib/Ic progenitor boundary suggests that such high velocities might also be present here.

To explore further the possibility that new ejecta dust was the source of the SN 2006jc NIR luminosity, we matched a simple dust IR emission model to the observed fluxes. The model is based on the escape probability formalism (Lucy et al. 1989; Osterbrock 1989; Meikle et al. 2007), in a spherical configuration. (The MIR component will be considered later.) An additional component was added to represent continuum emission from hot, optically thick gas in the ejecta. Details of this model are given in Meikle et al. (2007). We adopted a uniform dust density and temperature and investigated dust comprising either (i) pure amorphous carbon or (ii) pure silicates. The mass absorption functions were taken from the literature (Rouleau & Martin 1991; Laor & Draine 1993). The grain size distribution law was set at $m = 3.5$ (Mathis, Rumpl & Nordsieck 1977). The distribution limits were set at $a_{\rm min} = 0.005$ μm and $a_{\rm max} = 0.05$ μm, these being based on the typical grain size ranges calculated by Todini & Ferrara (2001) and Nozawa et al. (2003). The free parameters were the grain temperature, radius of the sphere and grain number density scaling factor. The model results are listed in Table 4. Between 55 and 121 d the sphere remained optically thick and expanded at a constant velocity of about 8500 $\pm$ 500 km s^{-1}. After this time, the observed fluxes could be reproduced by either reducing the expansion velocity or allowing the dust to become optically thin. We suggest that it is more likely that newly formed ejecta dust would expand steadily and so we fixed the expansion velocity at 8500 km s^{-1} for the latest three epochs.

For both grain materials, to match the *HK* fluxes up to about 100 d required a dust sphere expansion velocity of 7000–9000 km s^{-1} and also that the dust was optically thick at wavelengths up to at least 2.2 μm (Table 4). In practice we set the optical depth in the *K* band at about 2.5. For a Cardelli, Clayton & Mathis (1989) extinction law with $R_V = 3.1$ this corresponds to $A_V = 22$.

Table 4. Dust sphere model results for newly formed dust in the ejecta.

Epoch (d)	$M_{\rm dust}$ (10^{-4} M$_\odot$)	$\tau_{2.2\,\mu{\rm m}}$	Radius (10^{16} cm)	Temperature (K)
Amorphous carbon				
55	0.10	1.82	0.36	1800
64	0.23	2.40	0.48	1700
73	0.29	2.59	0.52	1800
76	0.30	2.44	0.55	1800
86	0.47	2.62	0.66	1760
93	0.60	2.85	0.72	1670
100	0.68	2.71	0.78	1570
114	0.67	2.44	0.82	1450
121	0.88	2.67	0.89	1370
176	0.62	0.90	1.29	1050
217	0.42	0.39	1.59	950
231	0.28	0.24	1.70	950
Silicates				
55	2.0	2.6	0.33	1850
64	2.5	2.6	0.51	1650
73	2.4	2.4	0.52	1800
76	3.0	2.4	0.55	1800
86	3.9	2.4	0.66	1760
93	4.6	2.4	0.73	1670
100	5.4	2.4	0.79	1570
114	6.0	2.4	0.84	1450
121	7.3	2.5	0.89	1370
176	5.3	0.88	1.29	1050
217	2.7	0.29	1.59	980
231	2.4	0.23	1.70	950

However, to achieve a match in the 55–100 d period required a temperature of 1600–1850 K for both amorphous carbon and silicate dust. Such high temperatures immediately ruled out silicates as the dust material (Smith et al. (2008) reached the same conclusion). For example, Todini & Ferrara (2001) find that while amorphous carbon grains form in the temperature range 1650–1900 K, for silicate grains the temperature must fall to 1100–1300 K before condensation occurs. This is consistent with the absence of the silicate feature in the vicinity of 8 μm at 228 and 430 d (see Fig. 3). Henceforth, we therefore focus our attention on amorphous carbon grains. Assuming that the expansion velocity remained at $\sim$8500 km s^{-1}, we found that the dust optical depth declined significantly by 176 d becoming optically thin (at 2.2 μm) by day 217. After 100 d, the temperature falls from $\sim$1500 to about 950 K by 231 d (see Table 4). The dust mass grew to $\sim 10^{-4}$ M$_{\odot}$ by day 121 and then declined to a third of this value by 231 d. The apparent decline in mass may be due to some dust cooling to below detectability in the *HK* bands. We conclude that a uniform amorphous carbon dust sphere can plausibly reproduce the NIR fluxes. As already indicated, the maximum expansion velocity is in line with the velocities seen in Type Ic nebular metal spectra. The maximum temperature is reasonable for amorphous carbon grain precipitation and the dust mass is modest.

The high optical depth might be seen as a problem as it would totally block out the optical emission from the ejecta. This seems to conflict with the much smaller estimated extinction (see above), but clumping of the ejecta could allow a sufficient fraction of the flux to escape to yield consistency with the extinction. One possible difficulty is the extraordinarily early appearance of the dust, namely $t \sim 50$ d. This contrasts with the well-studied SN 1987A where the earliest evidence of dust formation was at $\sim$350 d post-explosion (Meikle et al. 1993). This is consistent with the dust condensation calculations of Todini & Ferrara (2001) who found that the earliest dust (amorphous carbon) would appear at about 1 yr. However, recent calculations by Nozawa et al. (2008) suggest that such early dust condensation is possible in SN 2006jc (but see discussion in Section 5). A more serious difficulty is how to account for the attenuation of the narrow He I line red wings. If we accept that these lines are indeed due to a shell of material ejected at $\sim$2400 km s^{-1} in the LBV-like outburst of 2004 October then by epoch 121 d, when the maximum line shift was attained (see Fig. 6), the projected area of the putative ejecta dust sphere would be only $\sim$30 per cent of the projected shell and so would attenuate only the reddest 15 per cent of the red wing. In fact, almost the entire red wing had vanished by 140 d (see Fig. 5). Furthermore, there was no evidence for attenuation of the red wings of the broad SN lines that would have been expected if dust had formed within the ejecta. A similar argument has been made by Smith et al. (2008). We conclude that, in spite of the success of the ejecta dust sphere model in accounting for the observed IR emission, the spectral evidence argues against significant dust condensation in the ejecta.

4.4 An IR echo from pre-existing CSM dust?

We have argued that the IR behaviour of SN 2006jc strongly indicates the presence of dust in the SN vicinity. However, the strong blueshifts in the He I lines as well as, perhaps, the large radii of the blackbodies and the early appearance of the IR excess emission argues against newly formed dust in the ejecta. Nevertheless, the evolution of the He I spectral profiles and the behaviour of the individual light curves and quasi-BLCs (see Fig. 6) point to dust condensation taking place during an approximate 2–4 month period after the explosion. However, such dust may or may not also be responsible for the IR luminosity. We therefore first examine the latter possibility. Given the evidence that the progenitor of SN 2006jc was a massive, highly evolved star, we are prompted to explore the possibility that the bulk of the IR emission arose from pre-existing dust in the progenitor wind heated primarily by the early-time UV/optical emission from the SN, i.e. an IR echo.

The model used to test the IR echo hypothesis follows those of Bode & Evans (1980), Dwek (1983), Graham & Meikle (1986) and Meikle et al. (2006). A spherically symmetric dust cloud having a single grain size is adopted, with the actual value of the grain radius as a free parameter. UV/optical absorption and IR emission for the grains is calculated realistically using the emissivity function for amorphous carbon. Silicates are dismissed for the reasons given above (also see Dwek 1985). The input luminosity was a parametrized description of the *UBVRI* bolometric light curve of Pastorello et al. (2008a). To allow for the unobserved flux shortward of the *U* band, the luminosity was scaled up by a factor of about $\times 1.9$. The unobserved 0–22 d part was represented using a plausible extrapolation of the *UBVRI* BLC, namely $L_{\rm Bol} = 1.2 \times 10^{43} {\rm e}^{-t/84.4({\rm d})}$ erg s^{-1} (including the $\times$ 1.9 scaling). The later time IR excess light curves were not included in the input BLC for the following reason. For an IR echo from the pre-existing dust in the progenitor wind, owing to light traveltime, the resulting later time IR excess light curves would be dominated by the SN UV/optical luminosity around the time of peak emission. Valid addition of the IR light curves would therefore require them to be deconvolved from the light traveltime delays introduced by the echo process and the size of the dust-free cavity. We set the dust-free cavity radius to be 8×10^{16} cm (30 light-days), this being the distance from the SN at which the dust only just reaches the approximate evaporation temperature for amorphous carbon grains of 1800 K. For this size of cavity, the contribution of the appropriately deconvolved IR light curve to the UV/optical light curve would be small and so no attempt was made to include this small contribution to the BLC. The outer radius of the CSM was set at 10^{18} cm, although the actual value is not critical. We varied the grain radius, grain number density, CSM radial density law and the adopted characteristic wavelength of the input UV/optical radiation until the observed NIR SED and its evolution were reasonably reproduced. A grain radius of $a = 0.05$ μm, a $r^{-2.25}$ density law, and a characteristic input wavelength of 0.3 μm were settled upon. The dust mass is a modest 0.27×10^{-3} M$_{\odot}$, corresponding to a plausible CSM mass of $0.027 \times (0.01/r_{\rm dg})$ M$_{\odot}$ where $r_{\rm dg}$ is the dust-to-gas mass ratio. The UV/optical optical depth is low ($\tau \sim 0.056$) and so would not significantly attenuate the SN flux, in agreement with the low early-time extinction towards SN 2006jc of $A_V \leq 0.15$ (Pastorello et al. 2007). However, in order to match the observed NIR SED, it was also necessary to increase the input BLC luminosity by a further factor of $\times$ 3. Even taking into account the uncertainties in the SN distance and in the characteristic photon wavelength of the early-time BLC, plus the possibility of a contribution to the input luminosity by the IR component of the BLC at later times, such a factor does seem rather large. The need for the introduction of this factor suggests that a simple progenitor wind echo cannot account for the IR behaviour of SN 2006jc. Further evidence against this scenario is given below. In Fig. 7 we compare the echo model matches with the *H*- and *K*-band light curves (left-hand panel) and the 100- and 228-/31-d IR SEDs (right-hand panel). The NIR SEDs and the downward parts of the NIR light curves are well reproduced by the

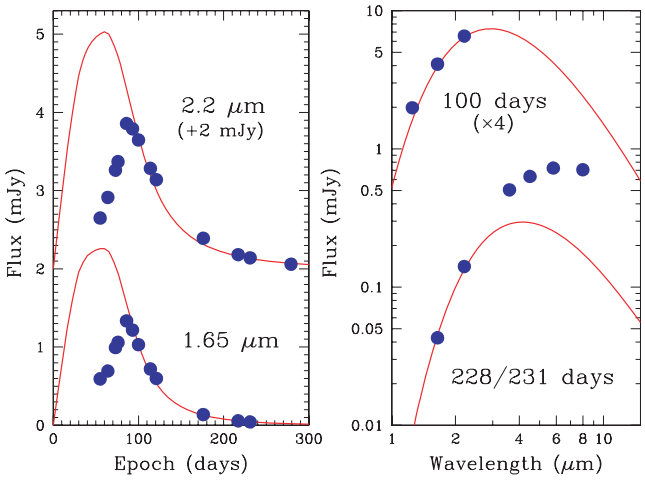

Figure 7. CSM wind IR echo model compared with the *H*- and *K*-band light curves of SN 2006jc (left-hand panel), and with the 100-d NIR SED and the 228-/31-d MIR SED (right-hand panel). The *K*-band light curve and the 100-d SED have been shifted vertically for clarity. The model parameters and their values are as follows. Grain type: amorphous carbon, grain material density: 1.85 g cm^{-3}, grain radius: 0.05 μm, emissivity law: $\lambda^{-1.15}$, CSM density law: $r^{-2.25}$, $r_{\rm in} = 8 \times 10^{16}$ cm, $r_{\rm out} = 10^{18}$ cm, $\tau_{\rm UV/optical} = 0.056$, dust mass: 0.27×10^{-3} M$_\odot$, CSM mass: $0.027 \times (0.01/r_{\rm dg})$ M$_\odot$, distance: 25.8 Mpc. To achieve the matches, the input SN BLC luminosity has been multiplied by 3. Also, note the failure of the model to reproduce (a) the delayed rise in the light curves and (b) the strong late-time MIR SED.

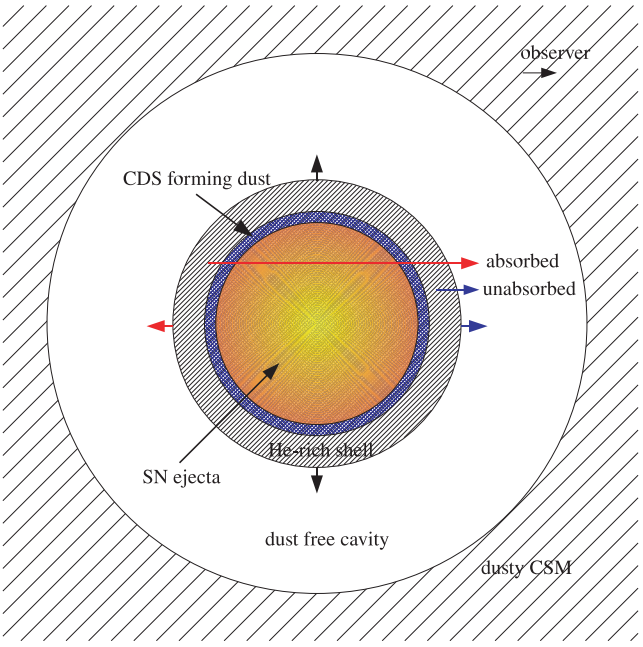

Figure 8. Schematic illustrating the geometry of the newly formed and pre-existing dust around SN 2006jc.

echo model. However, in addition to the rather implausible upward scaling of the input BLC, two other difficulties are apparent. One is that the model severely underproduces the MIR SED on day 228. The other problem is that the delayed rise in the IR light curve is not reproduced. While such a delay might be generated by placing the bulk of the dust on the far side of the SN, we regard this as an unattractive ad hoc solution.

We conclude that the pre-existing dust IR echo hypothesis is a rather implausible means of accounting for the overall IR behaviour of SN 2006jc. Moreover, such an explanation requires that the optical attenuation effects in the spectra and *UBVRI* light curves are due to a separate, newly formed, dust population which condensed early and quickly. However, as shown in Section 4.7, such an IR echo provides a good explanation for a significant and increasing proportion of the IR flux between 228 and 493 d.

4.5 Newly formed dust in the shocked CSM

We now consider the possibility that the bulk of the NIR emission was due to emission from dust lying much closer to the SN than the closest pre-existing dust that could have survived. To escape evaporation by the early-time SN luminosity, such dust would have to form *after* the peak luminosity had passed. The dust would then be able to condense within the dust-free zone surrounding the SN. Such a cavity could have been created by the SN peak luminosity or by a low mass-loss rate period during episodic progenitor mass-loss. The dust might be formed during the interaction of the ejecta with either a steady wind from the SN progenitor star or a dense shell of material ejected in a discrete event in the progenitor's past. It has been recognized for many years (e.g. Chevalier 1982) that the interaction of the SN with a dense CSM produces forward and reverse shocks. When radiative cooling is important at either shock front, the gas can undergo a thermal instability forming a dense, relatively cool zone, i.e. a CDS. Pozzo et al. (2004) invoked the formation of a CDS formed behind the reverse shock to explain the post-300 d IR excess observed in the Type IIn SN 1998S. In this case the CDS was composed mostly of ejecta material. In contrast, in the forward shock case the CDS forms primarily out of CSM material. If we assume a steady progenitor wind, the mass-loss rate from the progenitor star would need to be very high to produce a significant amount of dust. However, if the outward shock encounters a pre-existing dense circumstellar shell then, as pointed out also by Smith et al. (2008), substantial dust formation can take place with a much reduced net mass-loss from the progenitor. The latter case is pertinent to our SN 2006jc study since, as described above, a shell of circumstellar material was probably ejected during the LBV-like outburst seen 2 yr before the SN explosion. We therefore adopt the second scenario in the analysis that follows. This is illustrated in Fig. 8. As mentioned above, a dense shell behind the outward shock has already been invoked by Smith et al. (2008) and Di Carlo et al. (2008) as the main location for dust condensation in SN 2006jc (see Section 5 for further discussion).

To provide guidance for our interpretation of the IR luminosity within the shell context, we modelled the shock evolution. We propose that the ejecta impacted on the He-rich shell ejected during the LBV-like outburst in 2004 October and that a shock ran through the shell. During a significant fraction of the interaction time, the shock would have been radiative and dust could have condensed behind the shock. The LBV-like outburst occurred at about −730 d. Let us assume that the ejected shell expanded with a constant velocity of ∼2400 km s^{-1}, as suggested by the He I linewidths, up to the epoch of the earliest dust detection at 55 d. We know that the duration of the LBV-like outburst was no more than one month (see supplementary table 2 in Pastorello et al. 2007), implying a shell thickness of ≤4 per cent of the shell radius at the beginning of our observations. The interaction was therefore modelled assuming a thin-shell approximation. While this is valid for the radiative forward shock, the reverse shock propagating back into the SN ejecta will not be radiative and so the formation of a significant

CDS behind it is unlikely. Neither do we consider relativistic effects which could be important for the very early interaction with ejecta moving at velocities above $\sim$50 000 km s^{-1}. The structure of the shocked CSM shell was calculated using the same method as in Lundqvist & Fransson (1988), i.e. when the cooling time-scales are short compared with the hydrodynamical time-scales, the steady-state solution of the hydrodynamical equations can be solved using standard numerical techniques. These equations take into account spherical geometry. Ions and electrons are treated separately, with the energy exchange between these particles specified as in Spitzer (1962). Accurate radiative cooling is also calculated. This is carried out using a plasma code which calculates the ionization and emissivity as a function of electron temperature. All ionization stages of the elements were included, as well as all important types of emission (i.e. free–free emission, recombination emission, two-photon emission and line emission). The plasma code is described in some detail in Sorokina et al. (2004).

Following Model C of Pastorello et al. (2008a) and the models of Tominaga et al. (2008), we assumed an SN explosion energy of $\sim 10^{52}$ erg. The mass of the ejecta and the power-law index, n, of the presumed r^{-n} ejecta density profile of the outermost ejecta, were varied between 4 and 10 M$_\odot$, and between 8 and 12, respectively. The fastest ejecta expand at velocities in excess of $\sim$30 000 km s^{-1} and so would have reached the shell by 55 d when the IR excess was first observed. The ejecta were collided with a shell of CSM material expanding at 2400 km s^{-1} since the outburst in 2004, i.e. having an inner radius of 1.5×10^{16} cm at the time of the SN explosion, and 1.6×10^{16} cm at 55 d. For the calculations we adopted the following pre-SN surface abundances (by number): He:C:N:O = 0.90:0.060:0.003:0.037. These correspond to a WN/C transition object with an initial mass of 30 M$_\odot$ (assuming solar metallicity) (Eldridge & Vink 2006). We note that for a lower metallicity the initial mass of such a star would be larger while the pre-SN surface abundances would be roughly the same. For example, at an SMC metallicity the initial mass would be $\sim$50 M$_\odot$. In addition, we assumed that hydrogen was practically absent (at the level of 10^{-4} times the He abundance) and included Fe at 10^{-3} times the He abundance (by number).

An X-ray luminosity of $\sim 4 \times 10^{39}$ erg s^{-1} was observed for SN 2006jc (Immler et al. 2008) at $\sim$100–130 d. We found that a comparable X-ray luminosity can be produced using either an ejecta mass of $\sim$10 M$_\odot$ and a shell density of $\sim 3 \times 10^8$ cm^{-3} (henceforth Model 1), or an ejecta mass of $\sim$8 M$_\odot$ and a shell density of $\sim 5 \times 10^8$ cm^{-3} (Model 2). In both cases $n = 12$. For lower n and/or ejecta mass, the X-ray luminosity becomes too high at $\sim$100–130 d. A slightly lower ejecta mass of $\sim$5 M$_\odot$ was obtained by Pastorello et al. (2008a) and Tominaga et al. (2008) via BLC modelling. Our calculations show that in both Models 1 and 2, by 55 d a CDS is formed behind the forward shock. The mass of the CDS increases as the shock moves through the shell. By 120 d it is $\sim$0.18 M$_\odot$ in Model 1 and $\sim$0.40 M$_\odot$ in Model 2. The total mass of the swept-up CSM in the two models at 120 d is $\sim$0.58 and 0.53 M$_\odot$, respectively. As the shock moved through the shell, dragging along with it the shocked gas, the velocity of the CDS increased to $\sim$3000 km s^{-1} by 120 d in both Models 1 and 2. The shock temperatures in the two models are $\sim 0.9 \times 10^7$ and 1.2×10^7 K, respectively. By 120 d, ejecta at $\sim 1.7 \times 10^4$ km s^{-1} had reached the shell, while the outer edge of the CSM shell is at $\sim 1.8 \times 10^{16}$ cm. By this epoch, the shock was close to the outer limit of the CSM shell. At this stage it is likely that the CDS would be rather quickly accelerated by the ejecta, eventually being fragmented and dispersed. This provides a plausible explanation for the sudden drop in X-ray luminosity after 120 d (see Immler et al. 2008). By 120 d the mass of the CDS reached $\sim$0.2–0.4 M$_\odot$ in the two models discussed, corresponding to a cool carbon mass of $\sim$0.01–0.02 M$_\odot$ available to form new amorphous carbon dust within the CDS.

We then proceeded to investigate the possible IR emission from the CDS dust. How would such dust be heated? Between 55 and 231 d the IR energy released by the dust grains was $\sim 2 \times 10^{48}$ erg. The heat capacity of the grains is small and so the release of latent heat during the condensation plus the subsequent cooling would yield negligible IR emission. The ambient CDS gas would also contain insufficient thermal energy to provide the necessary heating of the grains. In contrast, there is more than enough energy in the shock itself to power the grain IR emission. Some of this energy might be coupled to the grains via the X-ray emission from the shock. However, the X-ray luminosity (Immler et al. 2008) is typically only $\sim$1 per cent of the NIR luminosity. Thus, it appears that the early-time UV/optical luminosity of the ejecta is the only plausible means of maintaining the NIR luminosity of the CDS grains. By day 230, the CDS radius was at least 2.0×10^{16} cm, i.e. the dust shell expanded from 6.0 to at least 7.7 light-days radius during the NIR observations. Even this minimum size of the shell is sufficient for light traveltime to affect the results. Therefore, we estimated the IR emission from the CDS dust using IR echo models similar to those described above. We note that in the past such IR echo models have only been used for pre-existing dust in the CSM and SN 2006jc thus provides the first case of an IR echo from newly formed dust within the CSM around an SN.

The thickness of the compressed CSM where the dust is formed is much less than the whole CSM shell thickness. Following calculations by Chevalier, Blondin & Emmering (1992) we adopted 1 per cent of the shell radius as the thickness of the dust-forming CDS. Prior to day 55, i.e. before there was significant shock interaction with the shell, the dust shell expansion velocity was assumed to be 2400 km s^{-1}, corresponding to a radius of 1.6×10^{16} cm at day 55. Between 55 and 120 d the CDS velocity was accelerated uniformly, reaching a velocity of 3000 km s^{-1}. Thereafter, the CDS was assumed to coast at 3000 km s^{-1}. However, as indicated above, the exact velocity and location of the CDS after the shock had passed through the CSM shell (at $\sim$120 d) is uncertain. There is likely to be a phase of acceleration and fragmentation, and so post-120-d radii are probably the lower limits.

The dust material was assumed to be amorphous carbon, having an emissivity law $\lambda^{-1.15}$. Given that the dust had recently formed, it was assumed that the grain size would be small (e.g. Nozawa et al. 2008). A grain radius of 0.005 μm was adopted. However, for grain radii less than about $\lambda/2\pi$, i.e. $< \sim$0.1 μm in this situation, the results are quite insensitive to the actual value chosen. The grain number density growth was represented by

$$n(t) = n_0\{1 - \exp[-(t - t_0)/t_\mathrm{d}]\},$$

where t is time, t_0 is the time at which dust condensation began, t_d is the characteristic grain growth time-scale and n_0 is the dust number density scaling factor. All times are as viewed from the SN. Thus, owing to the light traveltime differences, from the Earth the grain condensation is seen to commence during the epochs (t_0 − 6.0) to (t_0 + 6.0) d. Within the thin shell the dust number density was assumed to be uniform. The grains were assumed to appear instantaneously at their final size. No attempt was made to simulate the growth of individual grains, although this was probably fast once conditions were right (cf. a grain growth time-scale in ejecta of a few days: Todini & Ferrara 2001; Nozawa et al. 2003).

The source of energy for the echo is assumed to be the UV/optical radiation from the SN ejecta. For epochs beyond 22 d, we used a parametrized description of the blackbody-fit bolometric light curve of Pastorello et al. (2008a). The SN was unobserved during the 0–22 d period, but this is of no consequence here since this part of the SN emission had travelled well beyond the shell before grain condensation commenced. The parametrized BLC was scaled upwards by 15 per cent. This was to allow for the fact that by about 80 d the IR luminosity from the shell dominated the BLC. Consequently the observed BLC was delayed in the observer's time frame by about 6 d on average, compared with the SN frame. Thus, the 15 per cent enhancement has the effect of moving the light-curve time axis back by about 6 d. The SN itself was represented as a point source. Previously (Table 2) we found that even as early as 55 d, the hot component blackbody radius was only about 1 per cent of the shell radius. Thus, it is likely that the hot photosphere was small compared with the shell.

We found that the dust shell echo model, as described above, was able to reproduce the *K* light curve satisfactorily up to about 180 d. Moreover, the *H* light curve was also reasonably reproduced by the model (see Fig. 9). In addition, and of particular note, is that the rapidly declining equilibrium temperature for potential grains within the shell fell to 1900 K during the observation period 49–61 d (the range here being due to light traveltime across the shell) (see Fig. 9, right-hand panel). This is about the maximum condensation temperature of amorphous carbon grains. Thus the shell echo scenario yields a natural explanation for the particular epoch at which the NIR emission appeared. Prior to ∼50 d, the UV/optical light from the SN rendered the shell environment too hot for grains to form. We also found that the MIR SED at epochs 228 and 430 d, and the *K*-band 493-d flux were underproduced by the shell echo model. As with the blackbody study (Section 4.1) an additional cool component appeared to be present. While it may be possible to modify the CDS dust model so as to exhibit a range of dust temperatures (e.g. using a range of dust grain sizes, emissivities and densities) and so account for the cool, excess flux component, such an explanation would be rather ad hoc and have an unclear physical basis. Other possibilities are that the cool excess emission arose from (i) new dust formed in the ejecta or (ii) an IR echo from pre-existing dust in a circumstellar wind.

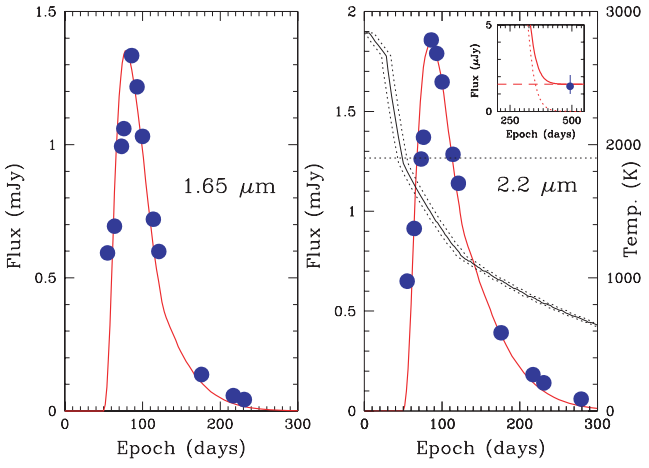

Figure 9. Comparison of SN 2006jc observed *H* and *K* light curves with the two-echo model. During the period shown in the main plots (0–300 d) the NIR fluxes are dominated by the shell emission. The inset in the right-hand panel shows a magnified plot of the model up to 550 d. The model is shown as a solid line, while the shell and wind components are shown as dotted and dashed lines, respectively. It can be seen that the 493-d *K*-band flux is dominated by the flux from the CSM wind. Also shown in the right-hand panel (plots descending from top left-hand side) is the equilibrium dust temperature. The three plots (going left- to right-hand side) indicate the temperature at the near side (dots), half-way (solid line) and the far side (dots) of the shell. The horizontal dotted line indicates a temperature of 1900 K, at which the condensation of amorphous carbon grains might be expected to begin. This corresponds to the observation epoch days 49–61.

4.6 The source of the cool late-time excess emission

To examine the ejecta dust hypothesis for the cool excess IR emission, we added a uniform dust sphere model (see Section 4.3) to the day 231 shell model. We find that to reproduce the excess MIR flux, the dust sphere must be expanding with a velocity of at least 9000 km s^{-1}. For the 9000 km s^{-1} case, $T = 590$ K, the dust mass is 1.0×10^{-3} M$_\odot$ and the dust is optically thick, even in the MIR, i.e. the SED is essentially a blackbody. Good reproduction of the cool excess flux can also be obtained with similar masses of optically thinner dust at similar temperatures, but the expansion velocity has to be increased, reaching ∼20 000 km s^{-1} by the time the dust is optically thin in the MIR (although even at this velocity it is still optically thick in the optical/NIR region). Given that refractory elements might exist at velocities up to ∼8000 km s^{-1}, it is conceivable that newly formed optically thick ejecta dust could be responsible for the excess MIR flux. Such a flux would be powered by the radioactive decay. Assuming Model C of Pastorello et al. (2008a), and using the formulae reported by Valenti et al. (2008) (see also Clocchiatti & Wheeler 1997; Colgate et al. 1997) to find the deposited luminosity we find that the optically thick cool excess model luminosity corresponds to × 1.08 of the deposited energy, i.e. given the uncertainties, there is just about enough energy for the ejecta dust hypothesis for the MIR excess at this epoch. However, for ejecta to reach the shell by day 230 requires a velocity of just ∼10 000 km s^{-1}. Thus, the optically thick ejecta dust hypothesis implies that its boundary would be almost contingent with the inner boundary of the shell, and would totally block out emission from the ejecta and the back half of the shell. This raises the difficulty that the CDS dust has a temperature of 830 K at this epoch (see Fig. 9) and yet the enclosed, near-contingent surface responsible for the cool excess emission would have a temperature of just 590 K. A variation on the new ejecta dust hypothesis for the cool late-time emission might be that a reverse shock from the ejecta/He I interaction produced a second, inner CDS within the ejecta. However, given the high velocity and low densities involved, we think that such a shock would not produce a significant CDS. We conclude that the IR emission from ejecta dust is an unlikely origin for the cool late-time excess flux.

An alternative and arguably more natural explanation for the cool excess flux component is provided by the fact that the progenitor or its binary companion showed an LBV-like outburst shortly before the explosion of SN 2006jc. Such a progenitor system would also be expected to have undergone longer term mass-loss producing an extended circumstellar wind. Therefore, in addition to the IR echo from the CDS, we would also expect to see a more conventional IR echo from pre-existing dust in the wind. Indeed, it would be surprising *not* to see any IR echo at all from this region. Sakon et al. (2008) have already suggested that the MIR excess could be due to an IR echo from pre-existing CSM dust. We therefore added a second echo, from the progenitor wind, to the model.

4.7 The two-echo model

For the progenitor wind component of the two-echo model, a constant mass-loss rate was assumed so the density varied as r^{-2}. The dust material was assumed to be amorphous carbon with an emissivity law $\lambda^{-1.15}$. The input luminosity was again assumed to be the UV/optical radiation from the SN ejecta. However, after the formation of the shell dust, most of the luminosity reaching the wind dust would have been in the form of IR radiation, which would have been inefficiently absorbed by the wind dust. Therefore, to make a conservative allowance for this, the input luminosity was a parametrized description of just the *UBVRI* bolometric light curve of Pastorello et al. (2008a), As in Section 4.4, to allow for the unobserved flux shortward of the *U* band, the luminosity was scaled up by a factor of about $\times 1.9$, and the early unobserved portion represented using a plausible extrapolation of the *UBVRI* BLC (see Section 4.4). The characteristic wavelength of the input BLC radiation was assumed to be 0.5 μm.

For the CDS shell component of the two-echo model, the dust number density scaling factor, plus the dust condensation start time and time-scale were adjusted to obtain a match to the 55–231 d *K*-band light curve. For the wind component, the grain radius, dust number density scaling factor and the inner and outer radii of the CSM were adjusted to match the MIR excess flux and the *K*-band point on day 493. The model results are compared with the data in Figs 9 and 10. The model parameter values are summarized in Table 5.

We note that a fair match to the *H*-band light curve was obtained without further adjustment of the model. A range of wind parameter values and grain sizes allowed the wind component to reproduce the MIR excess flux on days 228 and 430 plus the day 493 *K*-band point.

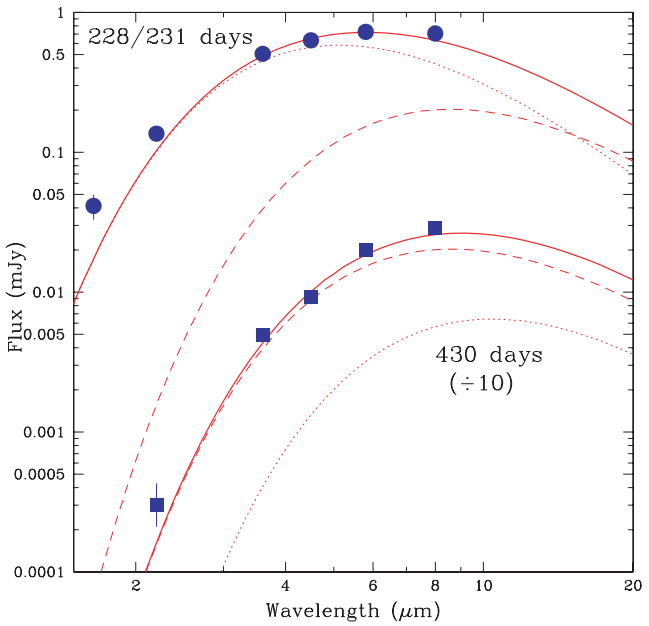

Figure 10. Comparison of SN 2006jc observed NIR/MIR SEDs on days 228/31 and 430 with the two-echo model. The model is shown as a solid line, while the shell and wind components are shown as dotted and dashed lines, respectively. For clarity, the day 430 model and data have been displaced downwards by a factor of 10. The *K*-band point at 430 d was obtained by interpolation between days 279 and 493. Owing to the uncertainty in this procedure an error of ±0.7 mag has been assigned to the interpolated point.

The inner radius, $r_{\rm in}$, could range from $\sim 6 \times 10^{17}$ cm (230 light-days) to $\sim 1.2 \times 10^{18}$ cm (460 light-days). The corresponding grain radii were from 0.16 μm down to 0.05 μm, while the corresponding total dust masses ranged from 8×10^{-3} to $25 \times 10^{-3}\,{\rm M}_{\odot}$. The model indicates that the evaporation radius would be about 0.8×10^{17} cm and so it is unlikely that this was the main cause of the cavity. Instead, we invoke episodic mass-loss. A large cavity due to episodic mass-loss was also inferred in the MIR study of SN 2002hh (Meikle et al. 2006). For $r_{\rm in} < 0.6 \times 10^{18}$ cm, while a match at 430/493 d could be achieved, the earlier NIR flux was increasingly overproduced. For $r_{\rm in} > 1.2 \times 10^{18}$ cm the dust temperature became too low to match the shape of the MIR SED. Also, above this radius the CSM mass became increasingly implausible ($M_{\rm CSM} > 5\,{\rm M}_{\odot}$). Satisfactory matches to the data could also be achieved with a range of wind outer radii, the main constraint here also being that the wind mass should stay within plausible bounds.

The shell dust mass at 230 d reached $0.3 \times 10^{-3}\,{\rm M}_{\odot}$, i.e. just a few per cent of the cool carbon mass available to form new amorphous carbon dust within the CDS (see above). If the dust mass continued to grow as specified by the exponential factor, it would asymptotically approach $0.44 \times 10^{-3}\,{\rm M}_{\odot}$. However, we have no evidence that the growth continued beyond 230 d. For the wind we give results for $r_{\rm in} = 7.5 \times 10^{17}$ cm and $r_{\rm out} = 30 \times 10^{17}$ cm, yielding a wind dust mass of $8.4 \times 10^{-3}\,{\rm M}_{\odot}$. This is close to the lower limit for the dust mass (see above). These dust masses correspond to gas masses of $0.03 \times (0.01/r_{\rm dg})\,{\rm M}_{\odot}$ in the shell (at 230 d) and $0.84 \times (0.01/r_{\rm dg})\,{\rm M}_{\odot}$ in the wind, where $r_{\rm dg}$ is the dust-to-gas mass ratio. For the pre-existing dust, the value is comparable to the dust and CSM masses found by Pozzo et al. (2006) and Meikle et al. (2006) for the Type IIP SN 2002hh. We note also that Morris et al. (1999) used *ISO* observations extending to 200 μm to infer $0.15\,{\rm M}_{\odot}$ of dust in the CSM of Eta Car. Thus, we consider the dust mass estimate for the SN 2006jc progenitor CSM as being entirely plausible. The UV/optical optical depths are 3.7 and 0.019 for the shell dust and CSM dust, respectively. The rather large optical depth of the shell is in agreement with the increase in the extinction of $A_V \sim 3$ estimated from the steepening of the optical light curves. It confirms that the shell must have been essentially opaque to UV/optical photons explaining the disappearance of the broad ejecta lines and the almost complete attenuation of the red wings of the He I lines. The low optical depth of the wind is in accord with the low extinction towards SN 2006jc. For the grain number density growth function, $t_0 = 50$ d and $t_{\rm d} = 160$ d. The quite large value of $t_{\rm d}$ is necessary to compensate for the rapid decline of the input SN light curve. This is, perhaps, a surprisingly long time given that it probably only took about 120 d for the shock to sweep through the shell. It may indicate that dust formation continued after the shock had departed the shell, or that the extent of the dust forming region was considerably greater than the 1 per cent of the shell radius that was adopted.

In summary, we note that having achieved a satisfactory match to the *K*-band light curve, the model spontaneously (i) generated an appropriate condensation temperature in the CDS at the right time and (ii) reproduced the *H*-band light curve. This was achieved using the actual SN bolometric light curve as input, an amorphous carbon emissivity, a simple grain number density growth scenario and a two-component spherically symmetric IR echo model. The MIR excess and the 493-d *K*-band point are satisfactorily reproduced by a dusty progenitor wind. Given the nature of the progenitor system, this seems entirely plausible. It seems unlikely that the cool excess IR emission arose solely from dust formed in the same CDS that

Table 5. Parameter values of the two-echo model.

Component	r_{in} (cm)	r_{out}	a (μm)	t_0 (d)	t_d (d)	τ_{UV-opt}	M_{dust} ($M_\odot$)
CDS[a]	20.7×10^{15}	20.9×10^{15}	0.005	50	160	3.7	0.3×10^{-3}
Wind	750×10^{15}	3000×10^{15}	0.13	–	–	0.019	8.4×10^{-3}

[a]The CDS shell radii, optical depth and dust mass are for the epoch 230 d.

produced the NIR emission. It is also unlikely that the cool excess emission was produced by newly formed ejecta dust powered by radioactive decay or by a reverse shock. In our view, a combination of IR echoes from the CDS dust and from a more extended dusty progenitor wind yield the most complete and convincing explanation for the IR behaviour of SN 2006jc.

5 DISCUSSION

Smith et al. (2008) find that only $0.6 \times 10^{-5}\,M_\odot$ of dust is needed to account for the NIR luminosity. At the epoch of their observations (95 d, our epoch definition) we find a shell dust mass of $1.1 \times 10^{-4}\,M_\odot$. We suspect that some of this factor of 18 discrepancy is due to the much larger grain radius, 0.3 μm, used by Smith et al. compared with our value of 0.005 μm. Inspection of Draine & Lee (1984) shows that for amorphous carbon, Q_v/a is about $\times 3.5$ larger at $a = 0.3$ μm radius than for $a < 0.03$ μm, and so the larger grain size will yield the same luminosity with less than 30 per cent of the mass. This is due to the increasing contribution of the magnetic dipole term to the emissivity as a increases above 0.03 μm. To our knowledge, grain growth calculations for an SN-shocked circumstellar shell have not yet been performed. However, we note that for grain growth in the SN ejecta environment the grain size is likely to be less than about 0.05 μm (e.g. Todini & Ferrara 2001; Nozawa et al. 2008). It therefore seems possible that the dust mass of Smith et al. required to account for the NIR luminosity is an underestimate. In addition, a grain size as large as 0.3 μm might not produce even the modest reddening within the optical region indicated by the optical light curves (Section 4.2).

Smith et al. (2008) also suggest that the total dust mass produced in the CDS over a time-scale of 2 months could be as high as 1 per cent of a solar mass or more, assuming that only the very hottest dust was detectable in the NIR. Our modelling (see Section 4.7) indicates that at 150 d, the mass of newly formed dust in the shell required to account for the NIR flux is about $2 \times 10^{-4}\,M_\odot$ and the UV/optical depth is already around 2.5. As we point out in Section 4.7, this is consistent with the observed optical SN light-curve behaviour. However, having $\sim 0.01\,M_\odot$ of dust within the CDS would result in an enormous optical depth and the dust would totally block out the optical SN light. Furthermore, the hot dust would lie on the *inside* of the CDS (heated by the SN luminosity) and so the NIR light would also be absorbed by the dust shell. However, as our observations show the SN remained detectable until ∼180 and 490 d at optical and NIR wavelengths, respectively. Therefore, we find such an enormous dust mass implausible.

Sakon et al. (2008), Tominaga et al. (2008) and Nozawa et al. (2008) invoke dust condensation in the ejecta to account for the NIR luminosity plus part of the MIR luminosity. Sakon et al. use a uniform, optically thin (in the NIR) dust sphere to estimate the dust mass and temperature at 220 d. While they do not indicate the size of this sphere, we find that, given their temperature of 800 K, the radius must be about 4.7×10^{16} cm. To reach this radius at 220 d would require a velocity of about 25 000 km s^{-1}. Even assuming an exceptionally massive progenitor for SN 2006jc, it seems rather unlikely that refractory elements will exist at this velocity. The very early appearance of dust might also be taken as an argument against ejecta dust formation, but modelling by Nozawa et al. (2008) suggests that about a solar mass of dust could have formed in the ejecta of SN 2006jc and that dust formation could have begun as early as 50 d. However, as they concede, it is difficult to see how effects such as clumping or destruction by high-energy photons/electrons could account for the much smaller (over three orders of magnitude) observed mass.

Nozawa et al. (2008) also argue that the LBV-ejected shell density would be too low for grains to nucleate. They base this on (i) the X-ray observations of Immler et al. (2008) and (ii) the hydrodynamic calculations of Tominaga et al. (2008). On the other hand, and as already pointed out in Pozzo et al. (2004) for SN 1998S and in Smith et al. (2008) for SN 2006jc, the physics of the CDS dust formation invoked here is reminiscent of the radiative shock of colliding winds of Wolf–Rayet stars which is known to be a dust-forming site (Usov 1991). Moreover, we have shown that a simple IR echo model involving new dust in a CDS and old dust in the progenitor wind can naturally account for the flux, the NIR/MIR SED and the evolution of the IR emission from SN 2006jc. As shown above, using an independently determined bolometric light curve and shell radius, the shape and rate of decline of the NIR flux are produced naturally within the IR echo scenario. In addition, the epoch predicted by the model at which dust condensation in the shell first becomes possible coincides with the epoch at which the NIR excess first appeared. These results give us confidence in the reality of the IR echo origin of the IR flux. Within their ejecta condensation model, Nozawa et al. find carbon dust condensation beginning at 40–60 d, but it is not clear how dependent this might be on the details of the sequence of hydrodynamic, nucleosynthesis and condensation model calculations upon which this result is based.

Smith et al. (2008) have argued against an NIR echo from pre-existing CSM dust on the basis of the grain temperature and its decay time-scale. However, we find that the temperature and decay time-scale could indeed be accounted for within a single, pre-existing dust IR echo scenario (see Fig. 7). In our view, the key objections to a pre-existing dust IR echo as the sole origin of the SN 2006jc IR behaviour are (i) the insufficient luminosity of the SN BLC, (ii) the delayed rise in the NIR light curves and (iii) the late-time MIR flux. Smith et al. have also argued that a pre-existing dust IR echo scenario would not account for the attenuation of the He I line profiles. We agree that this is true for an echo from an extended progenitor wind. We also agree that the CDS dust would be able to produce the observed He I profile evolution. As we show, an IR echo from this CDS dust can account for the bulk of the NIR emission from SN 2006jc. The dependence of the grain number density growth on its equilibrium temperature within the IR echo model also explains why the IR excess did not appear earlier. (The time it took for the SN shock to reach the shell probably also constrained the epoch at which dust was able to condense.)

6 CONCLUSIONS

The discovery of the IR excess in SN 2006jc has provided us with, for the first time, an opportunity to study in detail this phenomenon in an H-deprived SN. We have shown that the interaction of the ejecta outward shock with a dense shell of material ejected by the progenitor in an LBV-like outburst about two years prior to the SN explosion was able to produce a CDS behind the forward shock by 55 d from the explosion. The intensity, SED and evolution of the IR flux together with other evidence lead us to propose that this emission was due to IR echoes. The bulk of the NIR flux came from newly formed CDS dust while a substantial and growing fraction of the MIR flux came from pre-existing dust in the progenitor wind, probably lying beyond 6×10^{17} cm. The CDS amorphous carbon dust mass was $0.3 \times 10^{-3}\,M_{\odot}$ which is just a few per cent of the cool carbon mass of $\sim$0.01–0.02 $M_{\odot}$ at 120 d. This model explains the observed NIR evolution, as well as providing enough extinction ($A_V \sim 3$) to account for the fast decline in the optical light curves, the attenuation of the red wings of the CSM He I emission lines, and also the disappearance of the ejecta lines. The mass of pre-existing dust in the wind was at least $\sim 8 \times 10^{-3}\,M_{\odot}$. Given the $\sim 6 \times 10^{17}$ cm lower limit for $r_{\rm in}$ derived for the pre-existing CSM dust, and assuming a typical Wolf–Rayet star wind velocity of 1000 km s^{-1}, we can infer that the episodic mass-loss phase ceased at least $\sim$200 yr before the pre-SN outburst and the explosion of SN 2006jc. For the wind model results presented above (Table 5), the mass-loss would have taken place during the period 240–950 yr before the SN explosion, implying a mass-loss rate of $1.2 \times 10^{-3}\,(0.01/r_{\rm dg})\,M_{\odot}$ yr^{-1}. This is rather high for a Wolf–Rayet star (see e.g. Eldridge et al. 2006), adding weight to the proposition that SN 2006jc had an unusual progenitor.

The IR behaviour of SN 2006jc can be explained as a combination of IR echoes from two manifestations of stellar mass-loss and this paper provides two main conclusions. First, it adds to the growing evidence that mass-loss from the *progenitors* of CCSNe could be a major source of dust in the Universe. Secondly, we have witnessed dust formation in yet another type of CCSN. Furthermore, while dust condensation within the CDS formed behind the ejecta inward shock (in mainly ejecta material) has been proposed before for one event (SN 1998S), SN 2006jc is the first case with evidence for dust condensation in the CDS behind the ejecta outward shock in the circumstellar material. Finally, we note that two other events (SNe 1999cq and 2002ao) of the same Type Ibn class have also shown steepening optical light curves, similar to those of SN 2006jc. This suggests that CDS dust formation might well be a common characteristic in other events of this SN type (see also Smith et al. 2008 and Pastorello et al. 2008a). However, once again, we have seen no direct evidence that the explosion of an SN produces anything other than a very modest amount of dust.

ACKNOWLEDGMENTS

We thank an anonymous referee for useful comments and S. Valenti, L. Zampieri and D. Watson for helpful discussions. We also thank the Cambridge Astronomical Survey Unit (CASU) for access to the reduced UKIRT WFCAM images. This paper is based on observations made with the UKIRT, the *Spitzer* and the Gemini Observatory. UKIRT is operated by the Joint Astronomy Centre on behalf of the Science and Technology Facilities Council of the UK. The *Spitzer* is operated by the Jet Propulsion Laboratory, California Institute of Technology, under a contract with NASA. The Gemini Observatory is operated by the Association of Universities for Research in Astronomy, Inc., under a cooperative agreement with the NSF on behalf of the Gemini partnership: the National Science Foundation (United States), the Science and Technology Facilities Council (United Kingdom), the National Research Council (Canada), CONICYT (Chile), the Australian Research Council (Australia), CNPq (Brazil) and SECYT (Argentina). Financial support for this paper was provided by NASA through awards (30292, 40619) issued by JPL/Caltech. This paper, conducted as part of the award 'Understanding the lives of massive stars from birth to supernovae' made under the European Heads of Research Councils and European Science Foundation EURYI Awards scheme, was supported by the Participating Organizations of EURYI and the EC Sixth Framework Programme. SM acknowledges financial support from the Academy of Finland (project: 8120503).

NOTE ADDED IN PRESS

While our paper was in the proof preparation stage, Smith et al. (2008) appeared. In a note added in proof they suggest that our study (among others) showed that a 'pile-up' of a larger amount of cooler dust was indeed seen at longer infrared wavelengths, as they predicted in their Section 3.2. However, in Section 4.7 we show that the most plausible explanation for the mid-IR emission from SN 2006jc is an IR echo from pre-existing CSM dust. Moreover, in Section 5, we point out that such a large CDS dust mass is not consistent with the observations.

REFERENCES

Alard C., 2000, A&AS, 144, 363
Arkharov A., Efimova N., Leoni R., Paola A. D., Carlo E. D., Dolci M., 2006, The Astronomer's Telegram, 961, 1
Benetti S. et al., 2006, Cent. Bur. Electron. Telegrams, 674, 2
Bode M. F., Evans A., 1980, MNRAS, 193, 21P
Brown P. J., Immler S., Modjaz M., 2006, The Astronomer's Telegram, 916, 1
Cardelli J. A., Clayton G. C., Mathis J. S., 1989, ApJ, 345, 245
Cernuschi F., Marsicano F. R., Codina S., 1967, Ann. Astron., 30, 1039
Chevalier R. A., 1982, ApJ, 258, 790
Chevalier R. A., Blondin J. M., Emmering R. T., 1992, ApJ, 392, 118
Clocchiatti A., Wheeler J. C., 1997, ApJ, 491, 375
Colgate S. A., Fryer C. L., Hand K. P., 1997, in Ruiz-Lapuente P., Canal R., Isern J., eds, Thermonuclear Supernovae. Kluwer, Dordrecht, p. 273
Crotts A., Eastman J., Depoy D., Prieto J. L., Garnavich P., 2006, Cent. Bur. Electron. Telegrams, 672, 1
Danziger I. J., Gouiffes C., Bouchet P., Lucy L. B., 1989, IAU Circ., 4746, 1
Di Carlo E. et al., 2002, ApJ, 573, 144
Di Carlo E. et al., 2008, preprint (arXiv:0712.3855)
Draine B. T., Lee H. M., 1984, ApJ, 285, 89
Draper P. W., Gray N., Berry D. S., 2002, Starlink User Note 214.10
Dwek E., 1983, ApJ, 274, 175
Dwek E., 1985, ApJ, 297, 719
Dwek E., 1998, ApJ, 501, 643
Dwek E., Galliano F., Jones A. P., 2007, ApJ, 662, 927
Eldridge J. J., Vink J. S., 2006, A&A, 452, 295
Eldridge J. J., Genet F., Daigne F., Mochkovitch R., 2006, MNRAS, 367, 186
Elmhamdi A. et al., 2003, MNRAS, 338, 939
Elmhamdi A., Danziger I. J., Cappellaro E., Della Valle M., Gouiffes C., Phillips M. M., Turatto M., 2004, A&A, 426, 963
Fassia A. et al., 2000, MNRAS, 318, 1093
Filippenko A. V. et al., 1995, ApJ, 450, L11
Foley R. J., Smith N., Ganeshalingam M., Li W., Chornock R., Filippenko A. V., 2007, ApJ, 657, L105

Gehrz R. D., 1989, in Allamandola L. J., Tielens A. G. G. M., eds, Proc. IAU Symp. 135, Interstellar Dust. Kluwer, Dordrecht, p. 445
Gerardy C. L. et al., 2002, ApJ, 575, 1007
Graham J. R., 1985, PhD thesis, Univ. London
Graham J. R., Meikle W. P. S., 1986, MNRAS, 221, 789
Hendry M. A. et al., 2005, MNRAS, 359, 906
Hoyle F., Wickramasinghe N. C., 1970, Nat, 226, 62
Immler S., Modjaz M., Brown P. J., 2006, The Astronomer's Telegram, 934, 1
Immler S. et al., 2008, ApJ, 674, L85
Kennicutt R. C. Jr et al., 2003, PASP, 115, 928
Kotak R., Meikle W. P. S., Adamson A., Leggett S. K., 2004, MNRAS, 354, L13
Laor A., Draine B. T., 1993, ApJ, 402, 441
Lucy L. B., Danziger I. J., Gouiffes C., Bouchet P., 1989, in Tenorio-Tagle G., Moles M., Melnick J., eds, Lecture Notes in Phys. Vol. 350, Structure and Dynamics of the Interstellar Medium. Springer-Verlag, Berlin, p. 164
Lundqvist P., Fransson C., 1988, A&A, 192, 221
Matheson T., Filippenko A. V., Chornock R., Leonard D. C., Li W., 2000, AJ, 119, 2303
Mathis J. S., Rumpl W., Nordsieck K. H., 1977, ApJ, 217, 425
Minezaki T., Yoshii Y., Nomoto K., 2007, IAU Circ., 8833, 3
Meikle W. P. S., Spyromilio J., Allen D. A., Varani G.-F., Cumming R. J., 1993, MNRAS, 261, 535
Meikle W. P. S. et al., 2006, ApJ, 649, 332
Meikle W. P. S. et al., 2007, ApJ, 665, 608
Modjaz M., Blondin S., Kirshner R., Challis P., Matheson T., Mamajek E., 2006, Cent. Bur. Electron. Telegrams, 677, 1
Morris P. W. et al., 1999, Nat, 402, 502
Nakano S., Itagaki K., Puckett T., Gorelli R., 2006, Cent. Bur. Electron. Telegrams, 666, 1
Nozawa T., Kozasa T., Umeda H., Maeda K., Nomoto K., 2003, ApJ, 598, 78
Nozawa T. et al., 2008, ApJ, in press (arXiv:0801.2015)
Osterbrock D. E., 1989, Astrophysics of Gaseous Nebulae and Active Galactic Nuclei. University Science Books, Mill Valley, CA
Pastorello A. et al., 2007, Nat, 447, 829
Pastorello A. et al., 2008a, MNRAS, in press (doi:10.1111/j.1365-2966.2008.13602.x) (arXiv:0801.2277) (Paper I)
Pastorello A. et al., 2008b, MNRAS, in press (doi:10.1111/j.1365-2966.2008.13603.x) (arXiv:0801.2278) (Paper II)
Patat F., 1996, PhD thesis, Univ. Padova
Pozzo M., Meikle W. P. S., Fassia A., Geballe T., Lundqvist P., Chugai N. N., Sollerman J., 2004, MNRAS, 352, 457
Pozzo M. et al., 2006, MNRAS, 368, 1169
Rouleau R., Martin P. G., 1991, ApJ, 377, 526
Sakon I. et al., 2008, preprint (arXiv:0711.4801)
Smith N., Foley R. J., Filippenko A. V., 2008, ApJ, 680, 568
Sorokina E. I., Blinnikov S. I., Kosenko D. I., Lundqvist P., 2004, Astron. Lett., 30, 737
Spitzer L., 1962, Physics of Fully Ionized Gases. Interscience, New York
Sugerman B. E. K. et al., 2006, Sci, 313, 196
Suntzeff N. B., Bouchet P., 1990, AJ, 99, 650
Taubenberger S. et al., 2006, MNRAS, 371, 1459
Tielens A. G. G. M., 1990, in Tarter J. C., Chang S., Defrees D. J., eds, NASA Conf. Publ. 3061. NASA, Washington, DC, p. 59
Todini P., Ferrara A., 2001, MNRAS, 325, 726
Tominaga N. et al., 2008, preprint (arXiv:0711.4782)
Usov V. V., 1991, MNRAS, 252, 49
Valenti S. et al., 2008, MNRAS, 383, 1485

This paper has been typeset from a TEX/LATEX file prepared by the author.